Molecular Microbiology (2019) 111(2), 441–454
doi:10.1111/mmi.14165
First published online 5 December 2018

The toxin from a ParDE toxin–antitoxin system found in *Pseudomonas aeruginosa* offers protection to cells challenged with anti-gyrase antibiotics

Meenakumari Muthuramalingam,† John C. White, Tamiko Murphy, Jessica R. Ames and Christina R. Bourne*
The University of Oklahoma, Department of Chemistry and Biochemistry, Norman, 73019, OK USA.

Summary

Toxin-antitoxin systems are mediators of diverse activities in bacterial physiology. For the ParE-type toxins, their reported role of gyrase inhibition utilized during plasmid-segregation killing indicates they are toxic. However, their location throughout chromosomes leads to questions about function, including potential non-toxic outcomes. The current study has characterized a ParDE system from the opportunistic human pathogen *Pseudomonas aeruginosa* (Pa). We identified a protective function for this ParE toxin, PaParE, against effects of quinolone and other antibiotics. However, higher concentrations of PaParE are themselves toxic to cells, indicating the phenotypic outcome can vary based on its concentration. Our assays confirmed PaParE inhibition of gyrase-mediated supercoiling of DNA with an IC_{50} value in the low micromolar range, a species-specificity that resulted in more efficacious inhibition of *Escherichia coli* derived gyrase versus Pa gyrase, and overexpression in the absence of antitoxin yielded an expected filamentous morphology with multi-foci nucleic acid material. Additional data revealed that the PaParE toxin is monomeric and interacts with dimeric PaParD antitoxin with a K_D in the lower picomolar range, yielding a heterotetramer. This work provides novel insights into chromosome-encoded ParE function, whereby its expression can impart partial protection to cultures from selected antibiotics.

Accepted 25 October, 2018. *For correspondence. E-mail cbourne@ou.edu; Tel. (405) 325-5348; Fax (405)325-6111. †Present address: Department of Pharmaceutical Chemistry, University of Kansas, Lawrence, 66047, KS USA.

Introduction

Type II toxin–antitoxin (TA) systems, comprised of two non-secreted tightly interacting proteins, are encoded on plasmids as well as in bacterial and archaeal chromosomes (Makarova *et al.,* 2009; Yamaguchi *et al.,* 2011; Makarova *et al.,* 2013). Cellular proteases carry out a basal level of degradation of the toxin-neutralizing antitoxins (Brzozowska and Zielenkiewicz, 2013; Hayes and Kedzierska, 2014; Muthuramalingam *et al.,* 2016; Page and Peti, 2016). For some TA systems, the degradation is increased in response to specific classes of environmental stress (Christensen-Dalsgaard *et al.,* 2010). Toxin proteins can mediate alterations in bacterial metabolic activity when not neutralized by antitoxin, and the specific molecular targets underlie a classification system for different toxin families (Makarova *et al.,* 2009; Park *et al.,* 2013; Xie *et al.,* 2018). Our studies have focused on the ParE class of toxin, which is present throughout the *Firmicutes* and alpha- and gamma-*Proteobacteria* phyla.

Among the most prevalent toxin families is the RelE/ParE superfamily, which contains a conserved protein fold but, as typical for TA systems, has low sequence conservation (Anantharaman and Aravind, 2003; Pandey and Gerdes, 2005; Dalton and Crosson, 2010; Park *et al.,* 2013). The ParE toxins comprise a subfamily that has been demonstrated to inhibit gyrase-mediated supercoiling *in vitro* (Jiang *et al.,* 2002; Yuan *et al.,* 2010). This results in the accumulation of DNA breaks, promoting lethality in plasmid segregation killing (PSK) models, and thus invoking the SOS response *in vivo* (Jiang *et al.,* 2002; Hallez *et al.,* 2010; Yuan *et al.,* 2011). However, the chromosomal location of numerous ParDE operons raises questions about their roles in bacterial physiology (Roberts *et al.,* 1994). In *Vibrio cholerae*, three ParDE TA systems are located on accessory chromosome II where they maintain selection for this non-essential genetic component, similar to PSK (Yuan *et al.,* 2011). Four ParDE loci in *Caulobacter crescentus* can be activated in response to specific stresses, and it was noted that overexpression of these ParE toxins triggered a static rather than cidal growth state (Fiebig *et al.,* 2010). Studies on a unique tripartite ParE TA system

from *Escherichia coli* concluded that toxin activation is bactericidal (Hallez *et al.,* 2010; Sterckx *et al.,* 2016). For the ParDE2 system from *Mycobacterium tuberculosis*, a modest increase in survival after exposure to oxidative stress was noted in cells expressing the ParE toxin, indicating a protective rather than toxic effect (Gupta *et al.,* 2016). Therefore, it remains unclear if ParE toxins are part of a cohesive family with a unified role in cell physiology or if there are diverse subsets of ParE toxins with unique physiological outcomes (Sterckx *et al.,* 2016).

Other subfamilies of the RelE superfamily include the RelE, YoeB, and HigB toxins, which function as ribosome-dependent ribonucleases (Christensen and Gerdes, 2003; Christensen-Dalsgaard *et al.,* 2008; Hurley and Woychik, 2009; Zhang and Inouye, 2009). These toxins mediate selective metabolic reprogramming in response to cellular stress by altering the mRNA available for transcription (Christensen *et al.,* 2001; Christensen and Gerdes, 2004; Christensen *et al.,* 2004; Janssen *et al.,* 2015; Li *et al.,* 2016; Wood and Wood, 2016). The activity of these toxins has been linked to reversible inhibition of cellular metabolism, permitting subsequent re-growth after removal of the environmental stress, including treatment with bactericidal antibiotics (Page and Peti, 2016; Fisher *et al.,* 2017; Harms *et al.,* 2018; Song and Wood, 2018).

These types of metabolic changes may be relevant for the opportunistic human pathogen *Pseudomonas aeruginosa* (Pa), which is uniquely hardy to a wide variety of environmental conditions (Lutter *et al.,* 2008; Lister *et al.,* 2009; Moradali *et al.,* 2017). Adaptive survival is a known complication in Pa infections (Mulcahy *et al.,* 2010) and is positively correlated with antibiotic resistance across Pa strains (Balasoiu *et al.,* 2014; Cabot *et al.,* 2016; Vogwill *et al.,* 2016). While it remains tentative if TA systems are involved in dormant cell generation (Moradali *et al.,* 2017; Harms *et al.,* 2018), in general, TA systems are enriched in the genomes of clinical pathogens (Georgiades and Raoult, 2011; Fernandez-Garcia *et al.,* 2016). For Pa, a reliance on proteases such as Lon for survival under some antibiotic treatments provides indirect links to toxin effects, as toxins are expected to be activated upon proteolytic degradation of antitoxins by the Lon protease (Marr *et al.,* 2007; Breidenstein *et al.,* 2012; Fernandez *et al.,* 2012; Breidenstein and Hancock, 2013).

Despite the genetic heterogeneity of Pa clinical isolates (Lee *et al.,* 2006; Silby *et al.,* 2011), two TA systems, annotated as a RelBE and a HigBA, were expressed in all tested clinical isolates while a third TA system, a ParDE system, was present in a subset of isolates (Williams *et al.,* 2011). These three TA systems have also been predicted from bioinformatics studies as the most highly conserved TA systems in Pa strains (Pandey and Gerdes, 2005; Shao *et al.,* 2011). Further, a transcriptomics analysis previously identified variable expression of this annotated RelBE system in both clinical (fold-change between isolates of 2.4) and environmental samples (fold-change between isolates of 4.7) of Pa (Dotsch *et al.,* 2015). It is of note that findings of the current study indicate that this conserved annotated RelBE system is actually a ParDE-type TA system.

Recent studies on the HigBA system highlighted toxin-mediated effects on Pa cell physiology including a reduction of pyocyanin production and biofilm formation, as well as decreases in parameters of motility (Wood and Wood, 2016). Further studies derived an association of this HigBA system and the Type III Secretion System expression (Li *et al.,* 2016); neither study noted an effect on the viability or dormancy of Pa cultures. Given the implication of TA systems in altering cell physiology, the current study focused on the other highly conserved TA system from Pa, previously annotated as a RelBE, with the goal of investigating its predicted function and impact on the cell as a ParE-related family member. This annotated RelBE TA system is found at operon 0124–0125 in the Pa PA01 strain (Pandey and Gerdes, 2005; Williams *et al.,* 2011). Initial examination revealed a stronger structural similarity to the ParE-type toxin subfamily than the RelBE system, and our reported *in vitro* and *in vivo* experiments confirm this toxin is a functional chromosomally encoded ParE toxin.

Further, our investigations for the first time demonstrate a modest protective effect mediated by the ParE toxin when cultures were exposed to the bactericidal quinolone antibiotics ciprofloxacin (CIP) and levofloxacin (LEV), as well as to novoboicin (NOV), a different class of gyrase inhibitor. It was reasoned that this protective activity might be the result of interactions of both PaParE and the antibiotics with DNA gyrase. *In vitro* experiments indicate that PaParE-mediated and CIP-mediated DNA gyrase inhibition are relatively independent, with PaParE still able to inhibit gyrase until the concentration of CIP is above its IC_{50} concentration. At higher induction concentrations, PaParE mediates toxicity *in vivo* as a result of induced DNA damage, resulting in filamentous cell morphologies. Punctate staining for nuclear material further corroborated the mechanism of toxin interference with DNA topology in the cell. Therefore, ParE-mediated modulation of gyrase activity can promote the survival of cells exposed to gyrase-inhibiting antibiotics, while higher concentrations of ParE result in cell death. This is consistent with the idea of multiple cellular outcomes as a result of ParE toxin function. These data provide a first example of a TA-derived toxin that can exert either protective or toxic effects, depending on the amount of toxin present. This is expected to prove useful for studies aimed at harnessing the therapeutic potential of TA systems, as controlling expression levels will allow for selective promotion of survival or cell death.

Results

Gene pa0124 encodes a ParE-type rather than a RelE-type toxin based on structural homology, including a lack of catalytic amino acids for RNA degradation

From the amino acid sequence, it is apparent that the *pa0124* gene has a predicted conserved secondary structure consistent with the RelE superfamily (Fig. 1A). A threading homology model was constructed using the Swiss-Model online server (Biasini *et al.,* 2014). This protocol identified the closest matching template as 20% identical (31% similar) to *E. coli* ParE2 from a unique chromosomal three-component ParDE module (PDB ID 5CW7) (Sterckx *et al.,* 2016). Superposition of this model with the other known ParE structures (PDB IDs 5CW7, 3KXE, and 5CEG) (Dalton and Crosson, 2010; Aakre *et al.,* 2015; Sterckx *et al.,* 2016) and an *E. coli* RelE toxin structure (PDB ID 4FXI) (Boggild *et al.,* 2012) demonstrates the remarkable conservation of structure (Fig. 1B). However, the catalytic residues used by RelE to degrade RNA (highlighted in Fig. 1A and amino acid side chains shown as sticks in Fig. 1B) are absent in the *pa0124* sequence (Neubauer *et al.,* 2009; Dunican *et al.,* 2015; Schureck *et al.,* 2016). Of note are the longer helices predicted for the protein encoded by *pa0124,* consistent with other known structures of ParE toxin members but absent from RelE members (Fig. 1B). It was recently demonstrated that the shorter helix-turn-helix motif found in RelE-type toxins makes contacts with RNA in the ribosome (Maehigashi *et al.,* 2015), and our analysis supports that the longer helices found in ParE toxins would sterically hinder this interaction. The limited sequence

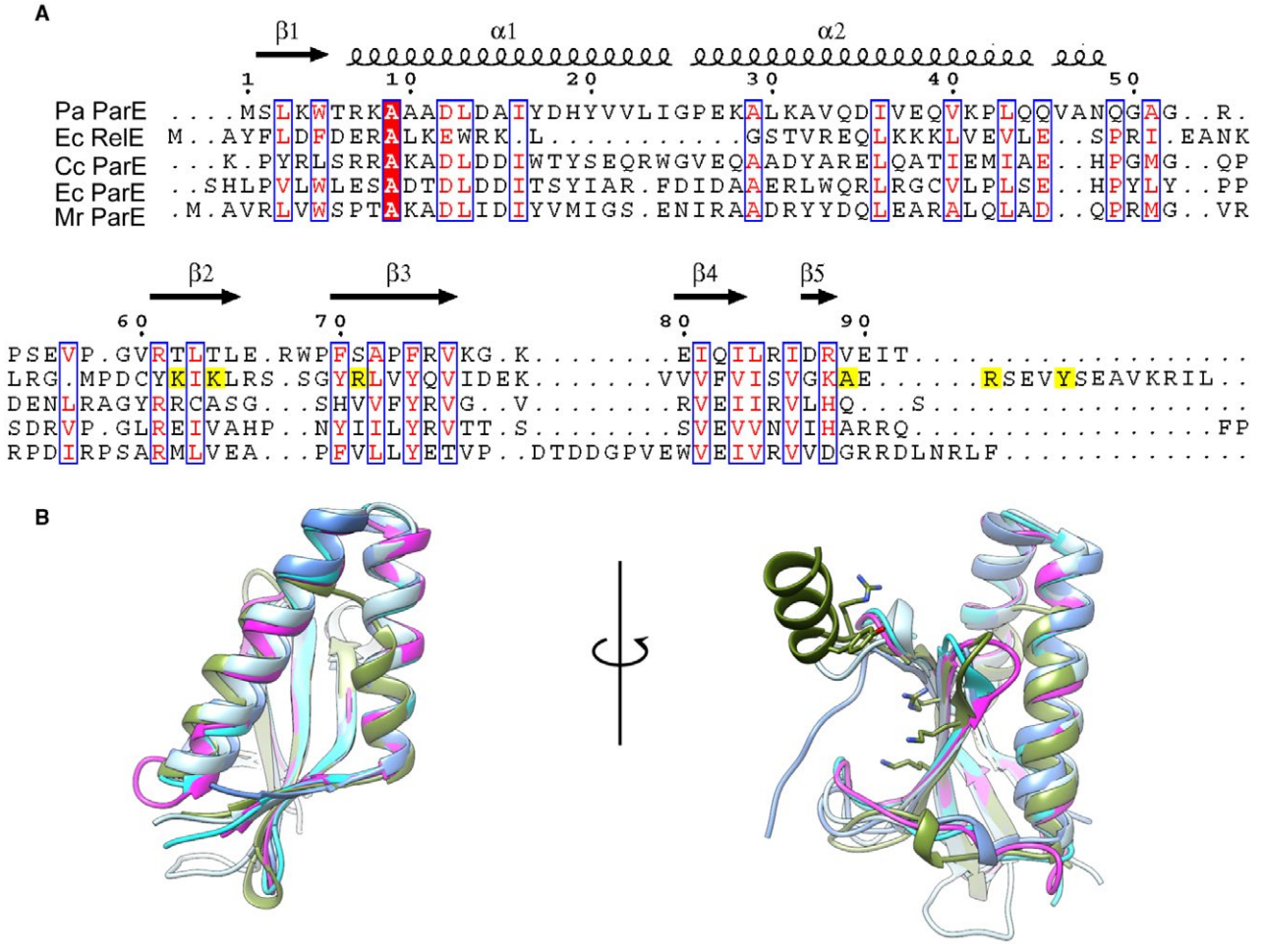

Fig. 1. The protein encoded by *pa0124* is predicted to have a structure consistent with other gyrase-inhibiting ParE toxins.
A. Secondary structure elements, highlighted above the sequence alignment, as well as amino acids integral to the fold of the protein (blue boxes) are conserved within the RelE/ParE super-family. However, catalytic RelE toxin residues (yellow highlights) are not conserved in ParE toxins. B. The *pa0124* sequence was threaded onto a ParE toxin from *E. coli* with 20% identity/31% similarity (PDB ID 5CW7, cyan) using the Swiss-Model online server. Superpositions are the *pa0124* homology model (magenta), an *E. coli* RelE (PDB ID 4FXI, 5% identity/61% similarity, green), an *M. opportunism* ParE (PDB ID 5CEG, 14% identity/59% similarity, blue) and a *C. crescentus* ParE (PDB ID 3KXE, 15% identity/62% similarity, light blue); the RelE catalytic residue side chains are indicated as sticks.

conservation, even among ParE-type toxins, precludes defining regions responsible for its cellular activity, i.e., a surface with the potential to interact with DNA gyrase. However, it is clear from these analyses that the *pa0124* gene likely encodes a ParE-type toxin, which we herein refer to as PaParE.

PaParE inhibits DNA gyrase in vitro, and results in decreased cell viability and altered cell morphology

Recombinant PaParE was tested for its inhibitory effects on the supercoiling activity carried out by DNA gyrase from *E. coli* or from *P. aeruginosa* using an *in vitro* agarose gel-based assay (Fig. 2) (Yuan *et al.,* 2010; Gupta *et al.,* 2016). Incubation of DNA gyrase in the presence of a topologically 'relaxed' plasmid substrate and with purified PaParE toxin strongly inhibited the subsequent gyrase-mediated accumulation of supercoiled DNA. Additionally, upon toxin exposure, a linear form of DNA increasingly accumulates. An IC_{50} value was calculated by titrating increasing toxin and quantifying the resulting intensity of the agarose gel band corresponding to supercoiled DNA, which for *E. coli* gyrase was 3.7 ± 0.8 μM, while for gyrase from *P. aeruginosa* was 11.7 ± 1.5 μM (Fig. 2A and B). Control experiments utilized identical assay conditions with ciprofloxacin in the place of the PaParE toxin, and for both sources of gyrase the IC_{50} value was 0.18 ± 0.04 μg ml^{-1} (Fig. S1). The inclusion of the antitoxin binding partner, PaParD, with PaParE prior to the reaction results in comparable activity of gyrase as for PaParD alone, indicating that the PaParE interaction is stronger with its antitoxin than with its cellular target.

To assess the effects of gyrase inhibition *in vivo*, constructs expressing either PaParE or PaParD were transformed into *E. coli* cells. In these experiments, an *E. coli* host was chosen rather than Pa cells to minimize confounding effects resulting from endogenous antitoxin expression, a standard practice in studies of TA systems (Gupta *et al.,* 2016; Li *et al.,* 2016; Li *et al.,* 2016). PaParE or PaParD expression was induced by the addition of 0.02% or 0.2% arabinose (to titrate the expression levels) and monitored for growth by turbidity as well as for viability based on colony-forming units (CFU) (Fig. 3A and B). While there was no observed change in the optical density, there was a prominent decrease in viable cells of almost 3-log_{10} after 3 h expression but only at 0.2% inductant concentration (Fig. 3A and B). The consistency of optical density measurements between the samples implies a lack of toxicity; however, at the higher arabinose concentration a concomitant drop in CFU counts is noted. This is a hallmark of cell filamentation, wherein filaments scatter more light than a normal cell, yielding a single growth center but scattering more light proportionally. Consistent with this observation, overexpression of PaParE toxin promoted a filamentous phenotype and interfered with DNA segregation, resulting in accumulation of highly compact nuclear material as visualized by DAPI staining (Fig. 3C). In contrast, PaParD antitoxin or

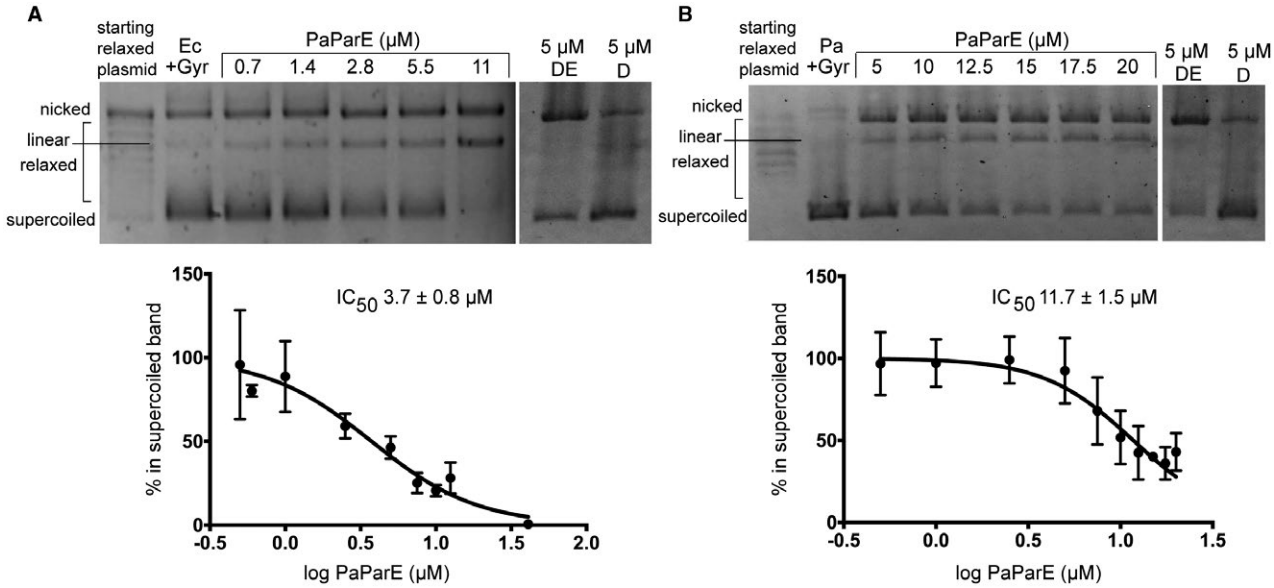

Fig. 2. PaParE is an inhibitor of DNA gyrase *in vitro.* (A, B) PaParE toxin causes an accumulation of linear DNA as supercoiling, produced from the starting relaxed plasmid by the action of DNA gyrase, is inhibited for both *E. coli* in A and *P. aeruginosa* gyrase B. Quantification of supercoiled DNA was plotted as a function of PaParE concentration to calculate IC_{50} values; data are from at least four independent measurements. Addition of the PaParD antitoxin to the PaParE toxin before initiating the reaction results in essentially the same pattern of gyrase activity as in the presence of PaParD alone for both *E. coli* and *P. aeruginosa* gyrase.

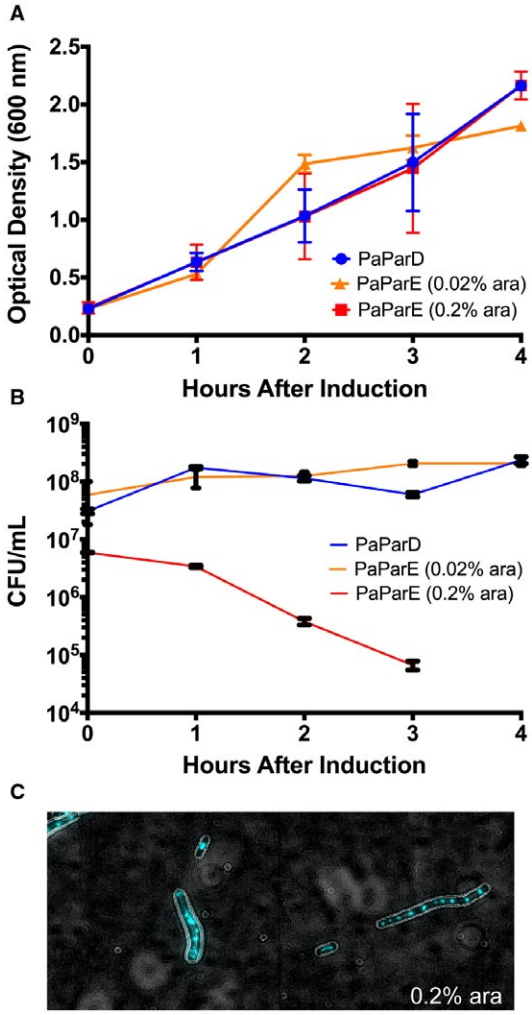

Fig. 3. PaParE toxin expression causes a decrease in cell viability and a filamentous morphology accompanied by punctate staining of nuclear material. Overexpression of PaParE toxin has A. no apparent effect on culture density, as measured at 600 nm, but B. causes a decrease in colony-forming units at higher induction. Overexpression of the PaParD antitoxin has no effect on density or CFUs. Data in A and B are from at least two biological replicates measured at least in duplicate. C. Overexpression of PaParE at higher induction (0.2% arabinose) causes a change in cell morphology, resulting in elongated filaments that exhibit punctate staining with DAPI (colored cyan), indicating multiple foci of accumulated nucleic acid within one elongated cell.

the expression vector without an inserted gene retained a normal phenotype and single spots of nucleic acid material per cell (Fig. S2).

PaParE expression confers modest survival to cells exposed to antibiotics

Quinolone antibiotics, particularly ciprofloxacin (CIP), are known to induce a tolerant phenotype at doses above the minimum inhibitory concentration (MIC) value (Dorr *et al.,* 2009); however, it is unknown if other DNA gyrase inhibitors, such as ParE toxins, could also induce a tolerant state. Based on the above results, cultures harboring the overexpression clones in *E. coli* were probed for the ability to survive in the presence of antibiotics using a disk diffusion method (Table 1). In addition, the experiment was performed with increasing amounts of gyrase-inhibiting antibiotics ciprofloxacin (CIP), levofloxacin (LEV), and the gyrase ATPase inhibitor novoboicin (NOV) (Table 2). In this experiment cells were plated after one hour of induction with 0.1% arabinose; bacterial growth occurs in a lawn except where zones of growth inhibition are mediated by antibiotics diffusing from placed disk material. For the culture overexpressing PaParE, susceptibility to the aminoglycosides tobramycin and gentamicin was essentially unchanged, as was susceptibility to chloramphenicol and nitrofurantoin (Table 1, Fig. S3). It is of note that the pHerd20T over-expression plasmid confers resistance to beta-lactams such as ampicillin, which was used as a control, as was Gram-positive specific vancomycin and water, all of which produced no differences in susceptibility (data not shown). Interestingly, the cephalosporin cefotaxime (30 μg), which interferes with cell wall synthesis, and the folate pathway inhibitor combination of trimethoprim-sulfamethoxazole were also less effective when PaParE was expressed. The protective response toward known gyrase inhibitors was measured using analogous methods but with increasing amounts of CIP, LEV and NOV in the disks. These studies resulted in a consistent 75–85% reduced zone of inhibition (Table 2, Fig. S4), indicating that the PaParE

Table 1. Disk diffusion experiments, calculated from averages of area measured in mm^2 and presented as the percent area of the zones of inhibition with PaParE expression relative to control samples.

Chloramphenicol (30 μg)	Gentamycin (10 μg)	Nitrofurantoin (300 μg)
100 ± 6	97 ± 5	100 ± 8
Tobramycin (10 μg)	Cefotaxime (30 μg)	Trimethoprim-sulfomethoxazole
92 ± 10	72 ± 8	78 ± 10

Data are from five independent biological replicates. Only changes in the area of growth in the presence of 30 μg cefotaxime and trimethoprim-sulfamethoxazole are statistically significant at $p < 0.05$.

Table 2. Dose-dependent disk diffusion experiments, calculated from averages of area measured in mm^2 and presented as the percent area of the zones of inhibition with PaParE expression relative to control samples.

	1 μg	5 μg	10 μg	25 μg
Ciprofloxacin	81 ± 8	81 ± 10	82 ± 11	82 ± 3
Levofloxacin	77 ± 3	86 ± 8	79 ± 13	82 ± 5
	50 μg	100 μg	250 μg	500 μg
Novobiocin	80 ± 7	79 ± 7	76 ± 31	61 ± 26

Data are from at least six independent biological replicates. All measurements are statistically significant at $p < 0.05$, except 250 μg and 500 μg novobiocin due to a larger variation in levels of inhibition.

toxin can diminish susceptibility to gyrase inhibitors with different molecular mechanisms and at a consistent level regardless of anti-gyrase antibiotic dose.

Combined PaParE toxin and ciprofloxacin mediated gyrase inhibition in vitro

Because anti-gyrase antibiotics such as CIP and the ParE toxins share a common molecular target, albeit with distinct mechanisms of target inhibition (Yuan *et al.,* 2010), it was reasoned that perhaps the toxin was able to directly protect DNA gyrase from inhibition by the quinolone CIP. To assess this, the *in vitro* supercoiling assay was again performed, but this time in the presence of both PaParE and CIP (Figs 4 and S5). When CIP is included in the reaction, inhibition results in the stabilization of individual topoisomers present in the starting relaxed plasmid DNA substrate (Mustaev *et al.,* 2014; Hooper and Jacoby, 2016). When the PaParE toxin is in the reaction, a linear form of DNA substrate accumulates (Figs 2 and 4). CIP or PaParE were added in the reaction at their respective IC_{50} values while the other inhibiting component was titrated, the evident products of the inhibited gyrase reaction are stabilized topoisomers, imparted by CIP inhibition, as well as an increase in the linear form mediated by PaParE (Fig. 4). This indicates that both inhibitors are able to function simultaneously. Above the IC_{50} value of either inhibitor its expected pattern of resulting DNA became the dominant species, suggesting that there was no direct competition at the inhibitor site.

To further probe the effects of co-incubation with inhibitors an order-of-addition experiment was performed. When CIP is added first very little changes are noted, as expected since CIP is known to trap an intermediate of gyrase-DNA. Preliminary experiments indicated that the *in vitro* gyrase assay is completed very quickly (less than 4 min.) upon incubation at 37 °C. In an effort to circumvent this and allow time for the PaParE toxin to act on DNA gyrase prior to adding CIP, the reactions were incubated at 23 °C for 5 min., CIP was added, and the reactions were incubated a further 25 min at 37 °C (Fig. 4C). While the activity of DNA gyrase is impaired by this even brief 23 °C incubation, there is a subtle reduction in the amount of DNA in the supercoiled form, meaning the inhibitors continued to demonstrate an additive inhibition. However, a noted lack of stabilized topoisomers when co-incubated with PaParE is also evident, highlighting an effect of PaParE when it is present before CIP is introduced. A table summarizing these findings is presented in Fig. 4D.

Monomeric PaParE toxin interacts strongly with dimeric PaParD antitoxin to form a heterotetramer

As a means to understanding the stoichiometry of this system, the individual PaParE toxin, PaParD antitoxin and the PaParDE complex were analyzed for oligomeric states in solution conditions using multi-angle light scattering (MALS). This revealed that the antitoxin exists as a dimer, the toxin molecule exists as a monomer and the complex exists as a heterotetramer composed of two antitoxins and two toxins (Fig. 5A). The strength of interaction between PaParE and PaParD was measured using Biolayer Interferometry with a 6 × His-tagged antitoxin immobilized and incubated with increasing concentrations of untagged PaParE toxin (Figs 5B and S6). Data were fit using a 1:1 model, resulting in R^2 values exceeding 0.99. The resulting values indicate a tight interaction with an apparent K_D value of 152 ± 12.8 pM as calculated from an on-rate of 7.5 × ± 0.3 10^5 M^{-1} s^{-1} and a slow off-rate of 1.2 ± 0.1 × 10^{-4} s^{-1}.

Discussion

Given the impact of TA systems in mediating growth changes that favor bacterial survival (Harms *et al.,* 2018; Song and Wood, 2018), the conserved TA systems in Pa are ideal for probing their functional roles. The protein encoded by *pa0124* was found to be of the ParE subtype, allowing correction of current annotation. Based on sequence and structural homology within the RelE superfamily, it is increasingly clear that certain distinguishing features, primarily the longer helices and lack of

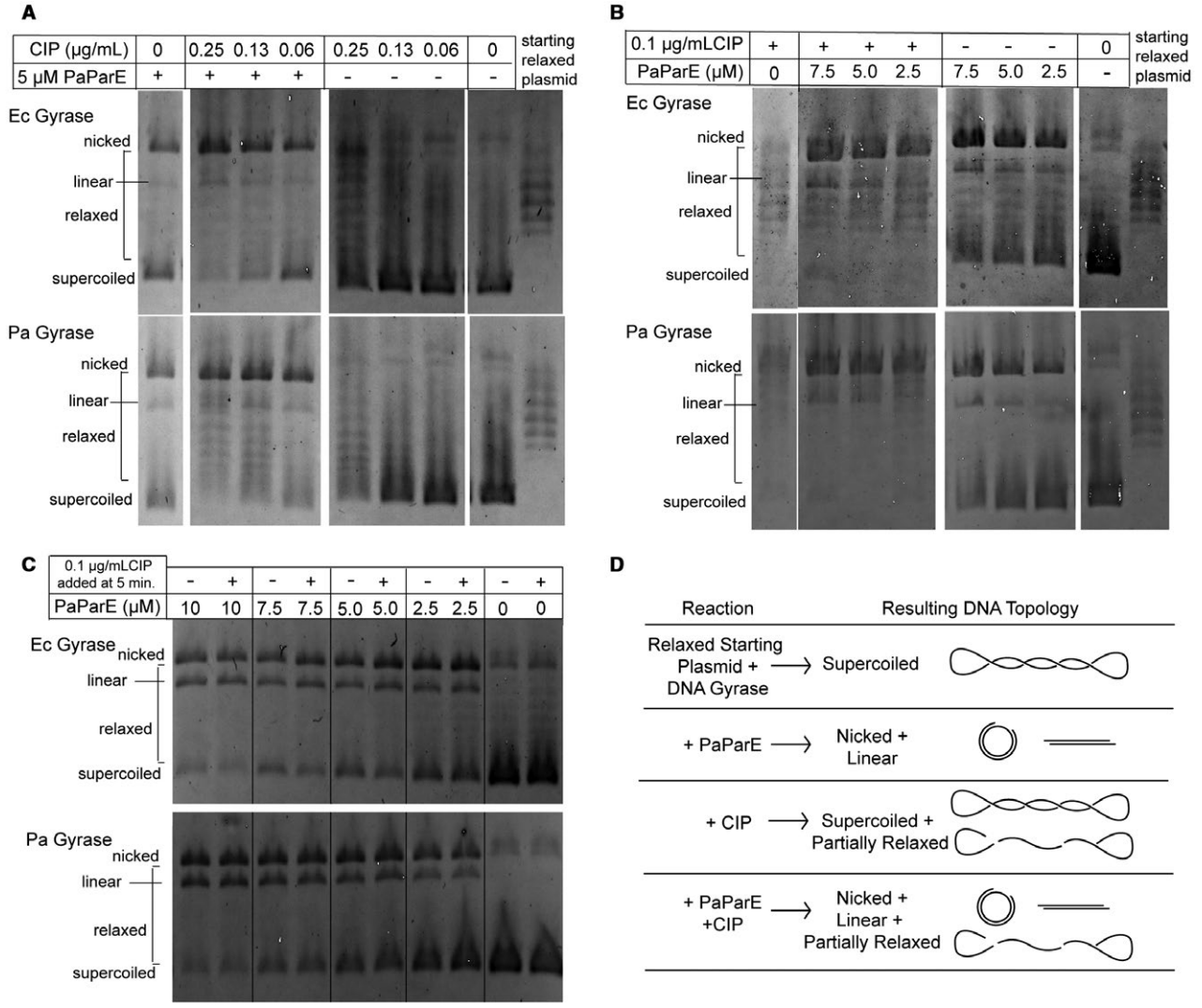

Fig. 4. PaParE and CIP can both mediate gyrase inhibition, such that PaParE is still active even in the presence of CIP. A. Titrating CIP with 5 μM PaParE (IC_{50} value for Ec gyrase), and B. titrating PaParE with 0.1 μg ml^{-1} CIP (IC_{50} value for gyrase), highlights the additive effect of the inhibitors, indicating both are active in the presence of each other. However, the prominent linear product produced by PaParE is present even at higher concentrations of CIP, while it is absent when CIP is the only inhibitor, indicating a slight dominant effect. (Also see Fig. S5). In both assays, the PaParE toxin and CIP were added at the same time. However, even if C. CIP is added up to 5 min after initiation of the reaction it is still able to elicit inhibition of gyrase (note the topoisomers in the + CIP samples with 5 μM toxin) until PaParE is present at a concentration above its IC_{50} value. While the extent of supercoiling is modestly affected by the addition of CIP, the intensity of the linear product is proportional only to the concentration of PaParE in the reaction. Representative gels shown; two to three independent experiments, performed in duplicate, yielded comparable results. D. Summary of the additive nature of the CIP and PaParE inhibitors as demonstrated by the resulting topologies of DNA when present in the *in vitro* DNA gyrase assay.

catalytic residues used for RNA degradation, are evident between RelE and ParE subtypes. In the future, consideration of these sequence features should allow more definitive identification of subfamily members based on sequence alone.

The toxicity observed *in vivo*, with a loss of ~3-log_{10} CFU ml^{-1}, in addition to microscopic observations of morphological changes to cell shape, are consistent with accumulating double-stranded (ds) DNA breaks. Previous reports on ParE toxins have identified a filamented morphological change when over-expressed in *E. coli* and attributed this to a cellular response to DNA damage (Fiebig *et al.,* 2010; Yuan *et al.,* 2011; Gupta *et al.,* 2016). These studies then confirm the identity of the *pa0124* gene product as a ParE-like toxin. This designation is also consistent with *in vitro* assays where incubation of PaParE with DNA gyrase revealed a loss of the supercoiled product and resulted in the accumulation of ds DNA breaks. Despite the loss of viable cells with higher

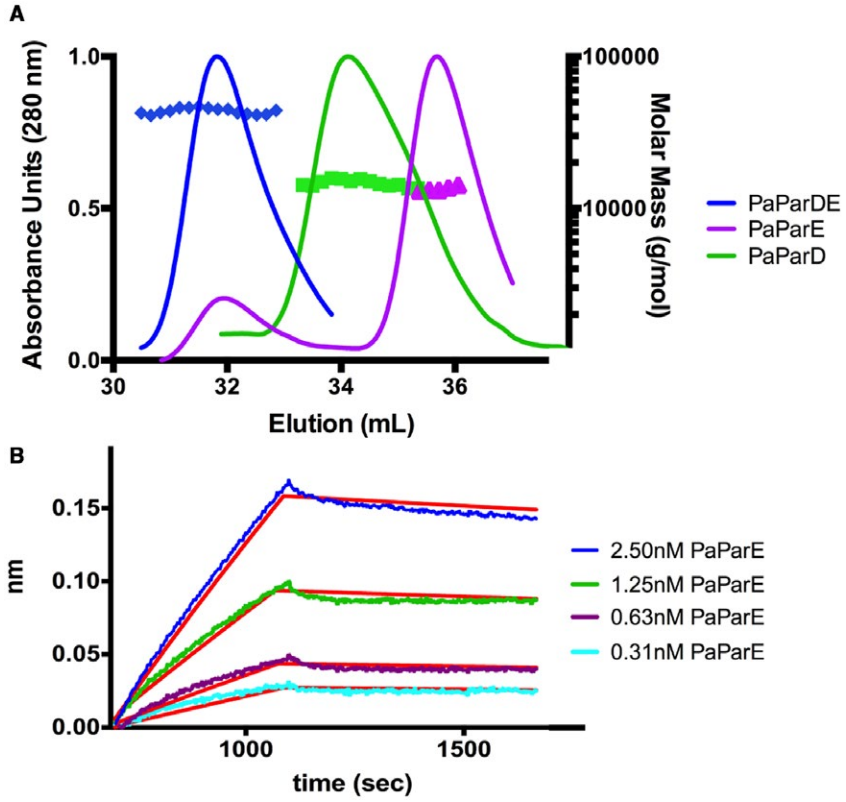

Fig. 5. The stoichiometry and strength of PaParE and PaParD interactions.
A. SEC-MALS analysis was used to determine that the complex of toxin (with no affinity tag) with antitoxin in solution, yielding a heterotetramer of 44,490 ± 1,077 Da. In addition, it was determined that the antitoxin PaParD forms a dimer of 14,740 ± 1,250 Da, and the affinity-tagged PaParE toxin exists as a monomer of 13,480 ± 635 Da.
B. The affinity of interaction of PaParD and PaParE was measured using Biolayer Interferometry by measuring the association ($7.5 \pm 0.3 \times 10^5$ M^{-1} s^{-1}) and dissociation ($1.2 \pm 0.1 \times 10^{-4}$ s^{-1}) of interaction as a function of varying PaParE concentrations. The resulting apparent K_D is 152 ± 12.8 pM; data shown are representative of four measurements (raw data are given in Fig. S6).

induction concentration, the culture density did not decrease. A similar observation was noted upon exposure to a ParE toxin from *Mycobacterium tuberculosis* and was interpreted as the formation of viable but non-culturable cells (Gupta *et al.,* 2016). However, the observation is also consistent from a change in the cell shape to a filamentous morphology, as interpreted in the current study. These responses have also been noted for other ParE toxins, as well as non-ParE toxins MazF (Cho *et al.,* 2017), RelE (Keren *et al.,* 2004) and HipA (Correia *et al.,* 2006) via altering protein synthesis (Jiang *et al.,* 2002). The quinolone CIP induces similar stressed states in *E. coli* both by inhibition of gyrase and also by activation of other TA systems, in particular the Type I TisB toxin found in K strains of *E. coli,* that inserts in the membrane and disrupts the proton motive force, as well as other TA systems responsive to SOS (Dorr *et al.,* 2010). Therefore, while ParE toxins are able to elicit specific cellular responses, the overall phenotypic outcome is shared among many other stressors.

The interaction strength of PaParE with PaParD is high, as expected for toxin–antitoxin pairs. For example, the strength of the toxin and antitoxin from the tripartite system from *E. coli* was K_D of 70 pM, comparable to our measurement of 152 pM for the PaParDE system. When PaParE is incubated with PaParD the inhibitory effect on DNA gyrase is blocked, indicating that the interaction with antitoxin is favored. In preliminary experiments, we have measured an interaction strength between PaParE and *E. coli* gyrase to be in the ~3 to 75 μM range by both isothermal titration calorimetry and surface plasmon resonance (data not shown). However, the interaction was complex with a biphasic character indicative of multiple binding events. Previous studies by others have identified a relatively tight interaction of a *Vibrio cholera* ParE with gyrase chain A (Yuan *et al.,* 2011), while a ParE derived from *Mycobacterium tuberculosis* was specific for gyrase chain B (Gupta *et al.,* 2016). Further, the tripartite ParE-containing system from *E. coli*, found most similar to PaParE for homology model construction, was noted to not interact with DNA gyrase (Sterckx *et al.,* 2016). Therefore, it is likely that the antitoxin would effectively compete with DNA gyrase *in vivo* for interaction with the PaParE toxin. The different potency of gyrase inhibition for

the *E. coli* versus *P. aeruginosa* gyrase is an interesting observation, and highlights that there may be sequence specificity such that more toxin protein is needed to inhibit the gyrase from its host species. This implies that the PaParE toxin is likely a protective rather than toxic mechanism in its native host, and should be borne in mind for future experiments characterizing toxin functions.

Earlier studies raised concerns about the possibility of gyrase-specific toxins, such as ParE, causing cross-resistance with quinolones, similar to the Qnr-type proteins (Ellington and Woodford, 2006). Subsequent studies demonstrated the independent nature of Qnr proteins from both the ParE toxin from broad host range plasmid RP4 as well as the CcdB toxin. Further, there was no change in the MIC of CIP when expression of the RP4 ParE toxin was induced using a low concentration of 0.005% arabinose, indicating a lack of protection (Kwak *et al.,* 2015). We surmise that the ParE toxin from RP4 has increased toxicity relative to PaParE, as in the previous study the RP4 ParE toxin was lethal when induced with 0.02% arabinose, which in our assays does provide a protective amount of PaParE. This may also be a distinguishing feature when comparing the plasmid-derived ParE toxins with those found in bacterial chromosomes. Our finding that lower induction of ParE toxin expression with 0.02% arabinose is not toxic is unexpected and reveals an opportunity for this toxin family to alter bacterial physiology. A dose-dependent toxicity, concomitant with a measurable effect on survival in antibiotics imparted by low toxin expression, is a unique finding that we predict is true for other chromosomal ParE toxin family members.

The inhibition mediated by the ParE toxin and CIP on DNA gyrase in the *in vitro* assay is distinct. This is consistent with a previous study of a ParE toxin from *Vibrio cholerae* that displayed the same activity when over-expressed in either wild-type or CIP-resistant *E. coli* cells (Yuan *et al.,* 2010). In our assays, it is also evident that CIP-mediated gyrase inhibition stabilizes a relatively even distribution of topoisomer species, while ParE-mediated gyrase inhibition produces decreases in supercoiled DNA species with concomitant increases in the nicked and linear DNA species. When both CIP and PaParE are present, the nicked DNA species still accumulates while the stabilized topoisomers are also still present. Therefore, when both inhibitors are added at the same time, the resulting pattern of inhibition appears to be additive; that is, there appears to be no interference of either inhibitor on the other's respective pattern of inhibition. Further, when PaParE is added first and CIP added 5 min into the reaction, a subtle reduction in the amount of supercoiled DNA is evident but without a dramatic stabilization of topoisomers. This implies there is some low level protection of the gyrase enzyme from CIP action that is mediated by the ParE toxin when it is present first. This is relevant for the interpretation of the culture-based studies, wherein cells can recover from lower concentrations of ParE inhibition but not necessarily from higher CIP concentrations.

The disk diffusion assay provided a measure of the protection from antibiotics afforded by PaParE expression, and this protection was consistent for each tested CIP, LEV or NOV dose, similar to what was previously found for other gyrase inhibiting proteins (Sengupta and Nagaraja, 2008; Sengupta *et al.,* 2008). This is particularly interesting as it argues against the direct protection of DNA gyrase by ParE, especially given that the quinolones and NOV have distinct and non-overlapping binding sites. However, no protection was noted upon exposure to the aminoglycosides tobramycin or gentamycin, or for ribosome-inhibiting chloramphenicol or the unclassified antibiotic nitrofurantoin. Interestingly, these assays revealed a comparable ParE-mediated protective effect upon challenge with folate pathway inhibitors trimethoprim-sulfamethoxazole (SXT) and with the cephalosporin class cefotaxime (CTX). SXT inhibition leads to a depletion of DNA precursors (Sangurdekar *et al.,* 2011; Capasso and Supuran, 2013), which may be why gyrase inhibition, and thus interruption of DNA replication, can afford protective benefits to SXT's effects. CTX inhibition leads to disruptions in membrane, which is not an obvious link to gyrase inhibition by ParE toxins. However, we have noted the accumulation of lipid-staining droplets at the poles of cells after ParE exposure (unpublished observation, manuscript in preparation), leading us to speculate that cells have a reduced requirement for, yet unaltered rate of, membrane synthesis when in the phenotypically filamented state.

We cannot exclude other factors that may have been triggered when the toxin was overexpressed, such as recent findings concerning phage contamination in deletion strains of *E. coli* responsible for the generation of persister cells (Harms *et al.,* 2017). It could be argued that the interaction of ParE toxin with gyrase could physically prevent or exclude further inhibition; however, our *in vitro* assays highlights that the CIP-mediated stabilization of relaxed topoisomers still occurs when lower concentrations of the PaParE toxin are present. Other recent studies identified 'density-dependent persistence', whereby stationary phase cultures are intrinsically tolerant to antibiotics including CIP due to a nutrient depletion that results in lowered metabolism (Gutierrez *et al.,* 2017). However, the current study investigated matched cultures, identical except for the induction of PaParE. Collectively, our data indicate that it is more likely that the PaParE toxin is able to interact with DNA gyrase and afford some protection from the effects of other inhibitors, and highlights the marked dependence on the relative concentrations of inhibitors. It remains unknown what concentrations would be inside the native *P. aeruginosa* host, and further studies are

needed to determine the extent of this effect in *P. aeruginosa*. The detailed molecular basis for the switch from protective effects at low concentrations to toxic effects at higher concentrations thus remains an important and active area for future study.

Experimental procedures

Construction of alignments and homology model

Percent identity and similarity were calculated using the online Sequence Manipulation Suite: Ident and Sim (Stothard, 2000) from secondary structure-guided sequence alignments produced in Chimera (Pettersen *et al.,* 2004). Sequence alignments were formatted with ESPript 3.0 (Robert and Gouet, 2014).

Recombinant plasmid construction and transformation

The *pa0125* gene and *pa0124* gene were PCR amplified (primers in Table S1), restricted and individually ligated into the pET-15b vector (Invitrogen) and the tightly controlled arabinose-inducible pHerd20T shuttle expression vector (Qiu *et al.,* 2008). Resulting constructs were verified by DNA sequencing. Transformation into *E. coli* strains utilized chemically competent cells (Table S1) and standard heat shock protocols; resulting strains were stored as glycerol stocks at −80 °C. Fresh inoculations from glycerol stocks were used in all experiments; throughout experimentation, expression plasmids from aliquots of cultures were periodically re-sequenced to ensure no accumulation of spontaneous mutations.

Toxicity assays

In order to observe phenotypic changes of the cells the plasmids encoding toxin and antitoxin in the pHerd20T vector were transformed into K strain *E. coli* NovaBlue DE3 cells (Novagen). The cultures were grown aerobically to an optical density of 0.2, induced with either 0.02% or 0.2% arabinose. After induction, optical density was monitored every hour, and samples were collected to determine the bacterial viability by serial dilution followed by plating on LB agar containing 0.2% glucose to repress further expression. Viable bacterial cells were counted and corrected for dilutions and amount plated, yielding colony forming units (CFU ml^{-1}).

Protein expression and purification

Escherichia coli BL21 DE3 pLys competent cells (New England Biolabs) containing the pET-15b::*pa0124* or::*pa0125* plasmid were grown in LB broth supplemented with 100 μg ml^{-1} carbenicillin and 0.2% glucose. Cultures were grown aerobically at 37°C to an optical density of 0.7–0.8 before induction with 0.5 mM IPTG for 2–8 h at 18 °C.

Cells were subsequently harvested and lysed in 100 mM Tris (pH 8.5), 300 mM NaCl using an Emulsiflex-C3 homogenizer (Avestin Inc); crude extract was centrifuged at 16000 × *g*, 4°C for 30 min. Clarified protein extract was applied onto a column pre-packed with Nickel-NTA resin (GE Healthcare or Roche) to capture the affinity tag, and eluted in 100 mM Tris (pH 8.5), 300 mM NaCl, supplemented with imidazole. Eluted fractions were combined and buffer exchanged into 100 mM Tris (pH 8), 150 mM NaCl, and the affinity tag was removed, when necessary, by incubation with thrombin (1 U mg^{-1}). After overnight digestion at 4°C the sample was re-applied to Nickel-NTA resin, the flow-through containing cleaved protein was captured and applied to a HiLoad 16/60 Superdex 75 pg column (GE Healthcare) equilibrated in 50 mM Tris (pH 8.5), 150 mM NaCl. Proteins were resolved on Tris-Tricine gels to assess their presence and purity (Schagger, 2006).

DNA gyrase supercoiling assay

Escherichia coli DNA Gyrase A and B subunits were purified essentially as described previously (Papillon *et al.,* 2013). The starting relaxed plasmid substrate was obtained by treating supercoiled pBR322 plasmid with Topoisomerase I (NEB) according to manufacturer's protocol. For some assays, commercial *E. coli* or *P. aeruginosa* DNA gyrase and relaxed pBR322 plasmid substrate were used (Inspirialis). The reaction mixture, which closely followed previously published methods (Yuan *et al.,* 2010; Gupta *et al.,* 2016), contained assay buffer (35 mM Tris·HCl (pH 7.5), 24 mM KCl, 4 mM $MgCl_2$, 2 mM DTT, 1.8 mM spermidine, 6.5% (w/v) glycerol, 0.1 mg ml^{-1} albumin), 500 ng relaxed pBR322 plasmid, 1 Unit of gyrase holoenzyme, and inhibitors (as required), in a total reaction volume of 30 μl. After incubation at 37 °C for 30 min the reaction was stopped by the addition of an equal volume of buffer containing 40% (w/v) sucrose, 100 mM NaCl, 100 mM Tris–HCl pH 8, 1 mM EDTA, 1% SDS. In experiments where CIP was added later, the reaction was incubated up to 5 min at room temperature prior to adding CIP, then incubated at 37 °C for the remaining 25 min. Samples were electrophoresed at 40 V (2 V/cm) for 4–5 h in 1% agarose gels, 1 × TAE, and subsequently stained with SYBR Safe (Invitrogen). Inhibition of DNA gyrase supercoiling activity was determined using the program ImageJ to quantify the intensity of the band for supercoiled DNA relative to the total lane intensity, and then normalized relative to positive and negative controls prepared and electrophoresed in the same experiment (Schindelin *et al.,* 2015). IC_{50} values were obtained by graphing the calculated percent of supercoiled DNA versus the amount of inhibitor (CIP or PaParE toxin), which was fitted to a four-parameter logistic equation in the program Graphpad Prism version 6.0d.

Visualization of cultures by microscopy

Samples were collected before induction and at four hours post-induction with 0.2% arabinose, washed twice in phosphate-buffered saline, and fixed with 70% ethanol. To observe morphological changes, the fixed cells were stained with safranin and images were captured at 100 × magnification with a standard light microscope. Additional aliquots of cells were applied to freshly prepared poly L-lysine coated slides,

and after 30 min unbound cells were removed by washing twice in phosphate-buffered saline. A coverslip containing 15 µl of 100 nM DAPI (4′,6-diamidino-2-phenylindole, dihydrochloride, Molecular Probes) was applied on the adherent cells and incubated for 5 min. Images were captured through a 100 × oil-immersion objective on an Olympus BX-50 microscope using a blue/cyan fluorescence filter.

Disk diffusion assay

Escherichia coli K strain NovaBlue DE3 cells carrying the pHerd20T constructs were grown overnight in sterile Luria-Bertani Miller (LB) media and the following morning re-inoculated at a 1:20 ratio. Cultures were then grown to early exponential phase, induced for 1 h with 0.1% arabinose, and swabbed evenly onto an LB agar plate containing the selection antibiotic (carbenicillin) and 0.1% arabinose. Antibiotic disks (Hardy Diagnostics) were placed using a sterile applicator, including those prepared in-house by pipetting known concentrations to 'blank' disks; plates were incubated at 37 °C for 16–18 h. Zones of inhibition were measured from digital images of plates using the Image Lab Touch Software v2.2 (Bio-Rad) and AntibiogramJ (Alonso *et al.,* 2017).

Size-exclusion chromatography coupled multi-angle light scattering

Purified samples of PaParDE, PaParD and PaParE were applied to a Superdex 200 Increase 10/30 GL column (GE Healthcare) and detected using both UV absorbance at 280 nm and light-scattering signal from a Wyatt miniDAWN Treos. Analysis of resulting signals utilized the ASTRA software version 6.1 (Wyatt Technologies).

Biolayer interferometry

Experiments were performed with an OctetRED96 system (ForteBio) using the manufacture's software for kinetic data collection, and results were processed using the manufacturer's software. All solutions were prepared to yield a final composition of 0.1 M Tris pH 8.0, 300 mM NaCl, 0.5% bovine serum albumin and 0.05% Tween-20. Purified samples of N-terminal 6×His-PaParD were prepared at 125 nM and incubated with Ni-NTA Biosensors (ForteBio). These sensors were then incubated with titrations of purified PaParE protein following proteolytic removal of the 6×His affinity tag. Concentrations of PaParE were adjusted to capture the dose-dependent responses, and dissociation reactions were measured for extended time points to increase the accuracy of the calculations. Control reactions utilizing empty biosensors were performed for each experiment to verify the absence of nonspecific binding between the PaParE toxin and the biosensor. Data were fit using a 1:1 Langmuir binding equation using the manufacturer-provided BioAnalysis software, version 8.2. Initial evaluation used a local fit protocol for each sensor; those with an R^2 value less than 0.95 were rejected and the remaining curves were used to perform a global fit with no mass transport correction. Four independent data sets (Fig. S6) were used to calculate average values.

Acknowledgements

We are grateful to Dr. Hongwei Yu (Marshall University) for the gift of the pHerd20T vector, Dr. Valentin Rybenkov and Bijit Bhowmik (University of Oklahoma) for access to and help with fluorescence microscopy, the Price Family Foundation Institute of Structural Biology for use of the Octet96 Biolayer Interferometry instrument, and Dr. Rakhi Rajan (University of Oklahoma) for access to the Multiangle Light Scattering equipment. We thank the University of Oklahoma Protein Production Core for assistance with protein expression and purification, and to Kevin Snead for help with protein preparations and binding interaction studies. We are indebted to the numerous mentors and lab staff that have contributed sage advice throughout these studies.

Conflicts of interest

The content is solely the responsibility of the authors and does not necessarily represent the official views of the National Institutes of Health. The authors declare that they have no conflicts of interest with the contents of this article.

Funding

Research reported in this publication was supported by an Institutional Development Award (IDeA) from the National Institute of General Medical Sciences of the National Institutes of Health under grant number P20GM103640, and in part through the award for project number HR17-099 from the Oklahoma Center for the Advancement of Science and Technology, and by start-up funds provided by the University of Oklahoma.

Author contributions

MM and CRB conceived the experiments. CRB prepared the data for Fig. 1, JCW and JRA performed initial experiments and CRB continued and analyzed experiments in Fig. 2, MM designed, performed and analyzed experiments in Fig. 3, CRB performed and analyzed experiments in Fig. 4, and TM and CRB performed and analyzed experiments in Fig. 5. MM and CRB wrote the manuscript, and all authors contributed revisions and approved the final version of this submission.

References

Aakre, C.D., Herrou, J., Phung, T.N., Perchuk, B.S., Crosson, S. and Laub, M.T. (2015) Evolving new protein-protein interaction specificity through promiscuous intermediates. *Cell*, **163**, 594–606.

Alonso, C.A., Dominguez, C., Heras, J., Mata, E., Pascual, V., Torres, C. *et al*. (2017) Antibiogramj: a tool for analysing images from disk diffusion tests. *Computer Methods and Programs in Biomedicine*, **143**, 159–169.

Anantharaman, V. and Aravind, L. (2003) New connections in the prokaryotic toxin-antitoxin network: relationship with the eukaryotic nonsense-mediated RNA decay system. *Genome Biology*, **4**, R81–R81.15.

Balasoiu, M., Balasoiu, A.T., Manescu, R., Avramescu, C. and Ionete, O. (2014) *Pseudomonas aeruginosa* resistance phenotypes and phenotypic highlighting methods. *Current Health Sciences Journal*, **40**, 85–92.

Biasini, M., Bienert, S., Waterhouse, A., Arnold, K., Studer, G., Schmidt, T. *et al*. (2014) SWISS-MODEL: modelling protein tertiary and quaternary structure using evolutionary information. *Nucleic Acids Research*, **42**, W252–W258.

Boggild, A., Sofos, N., Andersen, K.R., Feddersen, A., Easter, A.D., Passmore, L.A. *et al*. (2012) The crystal structure of the intact *E. coli* RelBE toxin-antitoxin complex provides the structural basis for conditional cooperativity. *Structure*, **20**, 1641–1648.

Breidenstein, E.B. and Hancock, R.E. (2013) Armand-Frappier outstanding student award – role of ATP-dependent proteases in antibiotic resistance and virulence. *Canadian Journal of Microbiology*, **59**, 1–8.

Breidenstein, E.B., Janot, L., Strehmel, J., Fernandez, L., Taylor, P.K., Kukavica-Ibrulj, I. *et al*. (2012) The Lon protease is essential for full virulence in *Pseudomonas aeruginosa*. *PLoS One*, **7**, e49123.

Brzozowska, I. and Zielenkiewicz, U. (2013) Regulation of toxin-antitoxin systems by proteolysis. *Plasmid*, **70**, 33–41.

Cabot, G., Zamorano, L., Moya, B., Juan, C., Navas, A., Blazquez, J. *et al*. (2016) Evolution of *Pseudomonas aeruginosa* antimicrobial resistance and fitness under low and high mutation rates. *Antimicrobial Agents and Chemotherapy*, **60**, 1767–1778.

Capasso, C. and Supuran, C.T. (2013) Sulfa and trimethoprim-like drugs – antimetabolites acting as carbonic anhydrase, dihydropteroate synthase and dihydrofolate reductase inhibitors. *Journal of Enzyme Inhibition and Medicinal Chemistry*, **29**(3), 379–387.

Cho, J., Carr, A.N., Whitworth, L., Johnson, B. and Wilson, K.S. (2017) MazEF toxin-antitoxin proteins alter *Escherichia coli* cell morphology and infrastructure during persister formation and regrowth. *Microbiology*, **163**, 308–321.

Christensen, S.K. and Gerdes, K. (2003) RelE toxins from bacteria and Archaea cleave mRNAs on translating ribosomes, which are rescued by tmRNA. *Molecular Microbiology*, **48**, 1389–1400.

Christensen, S.K. and Gerdes, K. (2004) Delayed-relaxed response explained by hyperactivation of RelE. *Molecular Microbiology*, **53**, 587–597.

Christensen, S.K., Mikkelsen, M., Pedersen, K. and Gerdes, K. (2001) RelE, a global inhibitor of translation, is activated during nutritional stress. *Proceedings of the National Academy of Sciences*, **98**, 14328–14333.

Christensen, S.K., Maenhaut-Michel, G., Mine, N., Gottesman, S., Gerdes, K. and Van Melderen, L. (2004) Overproduction of the Lon protease triggers inhibition of translation in *Escherichia coli:* involvement of the yefM-yoeB toxin-antitoxin system. *Molecular Microbiology*, **51**, 1705–1717.

Christensen-Dalsgaard, M., Overgaard, M., Winther, K.S. and Gerdes, K. (2008) RNA decay by messenger RNA interferases. *Methods in Enzymology*, **447**, 521–535.

Christensen-Dalsgaard, M., Jorgensen, M.G. and Gerdes, K. (2010) Three new RelE-homologous mRNA interferases of *Escherichia coli* differentially induced by environmental stresses. *Molecular Microbiology*, **75**, 333–348.

Correia, F.F., D'Onofrio, A., Rejtar, T., Li, L., Karger, B.L., Makarova, K. *et al*. (2006) Kinase activity of overexpressed HipA is required for growth arrest and multidrug tolerance in *Escherichia coli*. *Journal of Bacteriology*, **188**, 8360–8367.

Dalton, K.M. and Crosson, S. (2010) A conserved mode of protein recognition and binding in a ParD-ParE toxin-antitoxin complex. *Biochemistry*, **49**, 2205–2215.

Dorr, T., Lewis, K. and Vulic, M. (2009) SOS response induces persistence to fluoroquinolones in *Escherichia coli*. *PLoS Genetics*, **5**, e1000760–e1000768.

Dorr, T., Vulic, M. and Lewis, K. (2010) Ciprofloxacin causes persister formation by inducing the TisB toxin in *Escherichia coli*. *PLoS Biology*, **8**, e1000317.

Dotsch, A., Schniederjans, M., Khaledi, A., Hornischer, K., Schulz, S., Bielecka, A. *et al*. (2015) The Pseudomonas aeruginosa transcriptional landscape is shaped by environmental heterogeneity and genetic variation. *mBio*, **6**, e00749–e00758.

Dunican, B.F., Hiller, D.A. and Strobel, S.A. (2015) Transition state charge stabilization and acid-base catalysis of mRNA cleavage by the endoribonuclease RelE. *Biochemistry*, **54**, 7048–7057.

Ellington, M.J. and Woodford, N. (2006) Fluoroquinolone resistance and plasmid addiction systems: self-imposed selection pressure? *Journal of Antimicrobial Chemotherapy*, **57**, 1026–1029.

Fernandez, L., Breidenstein, E.B., Song, D. and Hancock, R.E. (2012) Role of intracellular proteases in the antibiotic resistance, motility, and biofilm formation of *Pseudomonas aeruginosa*. *Antimicrobial Agents and Chemotherapy*, **56**, 1128–1132.

Fernandez-Garcia, L., Blasco, L., Lopez, M., Bou, G., Garcia-Contreras, R., Wood, T. *et al*. (2016) Toxin-antitoxin systems in clinical pathogens. *Toxins*, **8**, 227–249.

Fiebig, A., Castro Rojas, C.M., Siegal-Gaskins, D. and Crosson, S. (2010) Interaction specificity, toxicity and regulation of a paralogous set of ParE/RelE-family toxin-antitoxin systems. *Molecular Microbiology*, **77**, 236–251.

Fisher, R.A., Gollan, B. and Helaine, S. (2017) Persistent bacterial infections and persister cells. *Nature Reviews Microbiology*, **15**, 453–464.

Georgiades, K. and Raoult, D. (2011) Genomes of the most dangerous epidemic bacteria have a virulence repertoire characterized by fewer genes but more toxin-antitoxin modules. *PLoS One*, **6**, e17962–e17971.

Gupta, M., Nayyar, N., Chawla, M., Sitaraman, R., Bhatnagar, R. and Banerjee, N. (2016) The chromosomal parDE2 toxin-antitoxin system of *Mycobacterium tuberculosis* H37Rv: genetic and functional characterization. *Frontiers in Microbiology*, **7**(886), 881–822.

Gutierrez, A., Jain, S., Bhargava, P., Hamblin, M., Lobritz, M.A. and Collins, J.J. (2017) Understanding and sensitizing density-dependent persistence to quinolone antibiotics. *Molecular Cell*, **68**(1147–1154), e1143.

Hallez, R., Geeraerts, D., Sterckx, Y., Mine, N., Loris, R. and Van Melderen, L. (2010) New toxins homologous to ParE belonging to three-component toxin-antitoxin systems in *Escherichia coli* O157:H7. *Molecular Microbiology*, **76**, 719–732.

Harms, A., Fino, C., Sorensen, M.A., Semsey, S. and Gerdes, K. (2017) Prophages and growth dynamics confound experimental results with antibiotic-tolerant persister cells. *mBio*, **8**, 768–784.

Harms, A., Brodersen, D.E., Mitarai, N. and Gerdes, K. (2018) Toxins, targets, and triggers: an overview of toxin-antitoxin biology. *Molecular Cell*, **70**, 768–784.

Hayes, F. and Kedzierska, B. (2014) Regulating toxin-antitoxin expression: controlled detonation of intracellular molecular timebombs. *Toxins*, **6**, 337–358.

Hooper, D.C. and Jacoby, G.A. (2016) Topoisomerase inhibitors: fluoroquinolone mechanisms of action and resistance. *Cold Spring Harbor Perspectives in Medicine*, **6**(9), a025320.

Hurley, J.M. and Woychik, N.A. (2009) Bacterial toxin HigB associates with ribosomes and mediates translation-dependent mRNA cleavage at A-rich sites. *Journal of Biological Chemistry*, **284**, 18605–18613.

Janssen, B.D., Garza-Sanchez, F. and Hayes, C.S. (2015) YoeB toxin is activated during thermal stress. *Microbiology Open*, **4**, 682–697.

Jiang, Y., Pogliano, J., Helinski, D.R. and Konieczny, I. (2002) ParE toxin encoded by the broad-host-range plasmid RK2 is an inhibitor of *Escherichia coli* gyrase. *Molecular Microbiology*, **44**, 971–979.

Keren, I., Shah, D., Spoering, A., Kaldalu, N. and Lewis, K. (2004) Specialized persister cells and the mechanism of multidrug tolerance in *Escherichia coli*. *Journal of Bacteriology*, **186**, 8172–8180.

Kwak, Y.G., Jacoby, G.A. and Hooper, D.C. (2015) Effect of Qnr on plasmid gyrase toxins CcdB and ParE. *Antimicrobial Agents and Chemotherapy*, **59**, 5078–5079.

Lee, D.G., Urbach, J.M., Wu, G., Liberati, N.T., Feinbaum, R.L., Miyata, S. *et al*. (2006) Genomic analysis reveals that *Pseudomonas aeruginosa* virulence is combinatorial. *Genome Biology*, **7**, R90.

Li, G., Shen, M., Lu, S., Le, S., Tan, Y., Wang, J. *et al*. (2016) Identification and characterization of the HicAB toxin-antitoxin system in the opportunistic pathogen *Pseudomonas aeruginosa*. *Toxins*, **8**, 113.

Li, M., Long, Y., Liu, Y., Liu, Y., Chen, R., Shi, J. *et al*. (2016) HigB of *Pseudomonas aeruginosa* enhances killing of phagocytes by up-regulating the type III secretion system in ciprofloxacin induced persister cells. *Frontiers in Cellular and Infection Microbiology*, **6**, 125.

Lister, P.D., Wolter, D.J. and Hanson, N.D. (2009) Antibacterial-resistant *Pseudomonas aeruginosa*: clinical impact and complex regulation of chromosomally encoded resistance mechanisms. *Clinical Microbiology Reviews*, **22**, 582–610.

Lutter, E.I., Faria, M.M., Rabin, H.R. and Storey, D.G. (2008) *Pseudomonas aeruginosa* cystic fibrosis isolates from individual patients demonstrate a range of levels of lethality in two *Drosophila melanogaster* infection models. *Infection and Immunity*, **76**, 1877–1888.

Maehigashi, T., Ruangprasert, A., Miles, S.J. and Dunham, C.M. (2015) Molecular basis of ribosome recognition and mRNA hydrolysis by the *E. coli* YafQ toxin. *Nucleic Acids Research*, **43**, 8002–8012.

Makarova, K.S., Wolf, Y.I. and Koonin, E.V. (2009) Comprehensive comparative-genomic analysis of type 2 toxin-antitoxin systems and related mobile stress response systems in prokaryotes. *Biology Direct*, **4**, 19–56.

Makarova, K.S., Wolf, Y.I. and Koonin, E.V. (2013) Comparative genomics of defense systems in archaea and bacteria. *Nucleic Acids Research*, **41**, 4360–4377.

Marr, A.K., Overhage, J., Bains, M. and Hancock, R.E. (2007) The Lon protease of *Pseudomonas aeruginosa* is induced by aminoglycosides and is involved in biofilm formation and motility. *Microbiology*, **153**, 474–482.

Moradali, M.F., Ghods, S. and Rehm, B.H. (2017) *Pseudomonas aeruginosa* lifestyle: a paradigm for adaptation, survival, and persistence. *Frontiers in Cellular and Infection Microbiology*, **7**, 39–67.

Mulcahy, L.R., Burns, J.L., Lory, S. and Lewis, K. (2010) Emergence of *Pseudomonas aeruginosa* strains producing high levels of persister cells in patients with cystic fibrosis. *Journal of Bacteriology*, **192**, 6191–6199.

Mustaev, A., Malik, M., Zhao, X., Kurepina, N., Luan, G., Oppegard, L.M. *et al*. (2014) Fluoroquinolone-gyrase-DNA complexes: two modes of drug binding. *Journal of Biological Chemistry*, **289**, 12300–12312.

Muthuramalingam, M., White, J.C. and Bourne, C.R. (2016) Toxin-antitoxin modules are pliable switches activated by multiple protease pathways. *Toxins*, **8**, 214–229.

Neubauer, C., Gao, Y.G., Andersen, K.R., Dunham, C.M., Kelley, A.C., Hentschel, J. *et al*. (2009) The structural basis for mRNA recognition and cleavage by the ribosome-dependent endonuclease RelE. *Cell*, **139**, 1084–1095.

Page, R. and Peti, W. (2016) Toxin-antitoxin systems in bacterial growth arrest and persistence. *Nature Chemical Biology*, **12**, 208–214.

Pandey, D.P. and Gerdes, K. (2005) Toxin-antitoxin loci are highly abundant in free-living but lost from host-associated prokaryotes. *Nucleic Acids Research*, **33**, 966–976.

Papillon, J., Menetret, J.F., Batisse, C., Helye, R., Schultz, P., Potier, N. *et al*. (2013) Structural insight into negative DNA supercoiling by DNA gyrase, a bacterial type 2A DNA topoisomerase. *Nucleic Acids Research*, **41**, 7815–7827.

Park, S.J., Son, W.S. and Lee, B.J. (2013) Structural overview of toxin-antitoxin systems in infectious bacteria: a target for developing antimicrobial agents. *Biochimica et Biophysica Acta*, **1843**, 1155–1167.

Pettersen, E.F., Goddard, T.D., Huang, C.C., Couch, G.S., Greenblatt, D.M., Meng, E.C. *et al*. (2004) UCSF Chimera–a visualization system for exploratory research and analysis. *Journal of Computational Chemistry*, **25**, 1605–1612.

Qiu, D., Damron, F.H., Mima, T., Schweizer, H.P. and Yu, H.D. (2008) pBAD-based shuttle vectors for functional analysis of toxic and highly regulated genes in *Pseudomonas* and *Burkholderia* spp. and other bacteria. *Applied and Environmental Microbiology*, **74**, 7422–7426.

Robert, X. and Gouet, P. (2014) Deciphering key features in protein structures with the new ENDscript server. *Nucleic Acids Research*, **42**, W320–W324.
Roberts, R.C., Strom, A.R. and Helinski, D.R. (1994) The parDE operon of the broad-host-range plasmid RK2 specifies growth inhibition associated with plasmid loss. *Journal of Molecular Biology*, **237**, 35–51.
Sangurdekar, D.P., Zhang, Z. and Khodursky, A.B. (2011) The association of DNA damage response and nucleotide level modulation with the antibacterial mechanism of the anti-folate drug trimethoprim. *BMC Genomics*, **12**, 583.
Schagger, H. (2006) Tricine-SDS-PAGE. *Nat Protocols*, **1**, 16–22.
Schindelin, J., Rueden, C.T., Hiner, M.C. and Eliceiri, K.W. (2015) The ImageJ ecosystem: an open platform for biomedical image analysis. *Molecular Reproduction and Development*, **82**, 518–529.
Schureck, M.A., Repack, A., Miles, S.J., Marquez, J. and Dunham, C.M. (2016) Mechanism of endonuclease cleavage by the HigB toxin. *Nucleic Acids Research*, **44**, 7944–7953.
Sengupta, S. and Nagaraja, V. (2008) YacG from *Escherichia coli* is a specific endogenous inhibitor of DNA gyrase. *Nucleic Acids Research*, **36**, 4310–4316.
Sengupta, S., Ghosh, S. and Nagaraja, V. (2008) Moonlighting function of glutamate racemase from *Mycobacterium tuberculosis*: racemization and DNA gyrase inhibition are two independent activities of the enzyme. *Microbiology*, **154**, 2796–2803.
Shao, Y., Harrison, E.M., Bi, D., Tai, C., He, X., Ou, H.Y. *et al.* (2011) TADB: a web-based resource for Type 2 toxin-antitoxin loci in bacteria and archaea. *Nucleic Acids Research*, **39**, D606–D611.
Silby, M.W., Winstanley, C., Godfrey, S.A., Levy, S.B. and Jackson, R.W. (2011) Pseudomonas genomes: diverse and adaptable. *FEMS Microbiology Reviews*, **35**, 652–680.
Song, S. and Wood, T.K. (2018) Post-segregational killing and phage inhibition are not mediated by cell death through toxin/antitoxin systems. *Frontiers in Microbiology*, **9**, 814.
Sterckx, Y.G., Jove, T., Shkumatov, A.V., Garcia-Pino, A., Geerts, L., De Kerpel, M. *et al.* (2016) A unique hetero-hexadecameric architecture displayed by the *Escherichia coli* O157 PaaA2-ParE2 antitoxin-toxin complex. *Journal of Molecular Biology*, **428**, 1589–1603.
Stothard, P. (2000) The sequence manipulation suite: JavaScript programs for analyzing and formatting protein and DNA sequences. *Biotechniques*, **28**(1102), 1104.
Vogwill, T., Comfort, A.C., Furio, V. and MaClean, R.C. (2016) Persistence and resistance as complementary bacterial adaptations to antibiotics. *Journal of Evolutionary Biology*, **29**, 1223–1233.
Williams, J.J., Halvorsen, E.M., Dwyer, E.M., DiFazio, R.M. and Hergenrother, P.J. (2011) Toxin-antitoxin (TA) systems are prevalent and transcribed in clinical isolates of *Pseudomonas aeruginosa* and methicillin-resistant *Staphylococcus aureus*. *FEMS Microbiology Letters*, **322**, 41–50.
Wood, T.L. and Wood, T.K. (2016) The HigB/HigA toxin/antitoxin system of *Pseudomonas aeruginosa* influences the virulence factors pyochelin, pyocyanin, and biofilm formation. *Microbiology Open*, **5**, 499–511.
Xie, Y., Wei, Y., Shen, Y., Li, X., Zhou, H., Tai, C. *et al.* (2018) TADB 2.0: an updated database of bacterial type II toxin-antitoxin loci. *Nucleic Acids Research*, **46**, D749–D753.
Yamaguchi, Y., Park, J.H. and Inouye, M. (2011) Toxin-antitoxin systems in bacteria and archaea. *Annual Review of Genetics*, **45**, 61–79.
Yuan, J., Sterckx, Y., Mitchenall, L.A., Maxwell, A., Loris, R. and Waldor, M.K. (2010) *Vibrio cholerae* ParE2 poisons DNA gyrase via a mechanism distinct from other gyrase inhibitors. *The Journal of Biological Chemistry*, **285**, 40397–40408.
Yuan, J., Yamaichi, Y. and Waldor, M.K. (2011) The three *Vibrio cholerae* chromosome II-encoded ParE toxins degrade chromosome I following loss of chromosome II. *Journal of Bacteriology*, **193**, 611–619.
Zhang, Y. and Inouye, M. (2009) The inhibitory mechanism of protein synthesis by YoeB, an *Escherichia coli* toxin. *Journal of Bacteriology*, **284**, 6627–6638.

Supporting Information

Additional supporting information may be found online in the Supporting Information section at the end of the article.